Nebulette is a powerful cytolinker organizing desmin and actin in mouse hearts

Daniel A. Hernandez[a,†], Christina M. Bennett[a,†], Lyubov Dunina-Barkovskaya[a], Tatjana Wedig[b], Yassemi Capetanaki[c], Harald Herrmann[b,d], and Gloria M. Conover[a,*]

[a]Department of Biochemistry & Biophysics, Texas A&M University, College Station, TX 77843-3474; [b]Division of Molecular Genetics, German Cancer Research Center (DKFZ), D-69120 Heidelberg, Germany; [c]Center of Basic Research, Biomedical Research Foundation Academy of Athens, Athens 11527, Greece; [d]Institute of Neuropathology, University Hospital Erlangen, D-91054 Erlangen, Germany

ABSTRACT **In the hearts of patients bearing nebulette mutations, a severe general disorganization in cardiomyocytes of the extrasarcomeric desmin intermediate filament system is frequently observed. However, the molecular and functional relationship between the desmin cytoskeleton and nebulette-containing sarcomeres is still unclear. Here we report a high-affinity in vitro interaction between nebulette and desmin filaments. A major interaction site has been mapped to the desmin α-helical rod domain, indicating that the filament core is directly involved in the binding of nebulette. The disease-mutant desmin variants E245D and T453I exhibited increased binding affinity for nebulette, delayed filament assembly kinetics, and caused significant weakening of networks. In isolated chick cardiomyocytes and sections from canine heart, we revealed by ground-state depletion and confocal microscopies that module 5 of nebulette extends outward from Z-disk–associated desmin filaments toward the center of the sarcomere. Accordingly, in the myocardium of Des$^{-/-}$ mice, elevated levels of cardiac actin correlated with alterations in the distribution of nebulette. Our data suggest that a well-organized desmin network is required to accommodate an optimal conformation of nebulette on sarcomeres to bind and recruit cardiac α-actin. Hence we propose that nebulette acts in synergy with nebulin to reinforce and temporally fine-tune striated muscle relaxation–contraction cycles.**

Monitoring Editor
Robert D. Goldman
Northwestern University

Received: Apr 18, 2016
Revised: Aug 31, 2016
Accepted: Oct 5, 2016

INTRODUCTION

Myofibers rely on the precise organization of their sarcomeres to generate and transmit force. The principal elements of sarcomere substructure, as observed by electron microscopy (EM), are the thin and thick filaments made from actin and myosin, respectively (Fawcett and Bloom, 1986). Actin filaments are anchored by their barbed ends at the Z-disks and intercalate with myosin filaments near their pointed ends. These in turn are connected at both ends by elastic titin molecules, the largest protein in muscle, exhibiting a length of 2 μm. Nebulin, the second-largest sarcomeric protein (~900 kDa), stabilizes a large core of the actin filaments (Chu *et al.*, 2016). In support of these long range–acting factors, nebulette, the smaller and functionally related protein, is thought to stabilize a shorter core of the actin filaments in cardiac cells (Littlefield and Fowler, 2008). Nebulin physically binds to desmin, the most abundant muscle-specific intermediate filament (IF) protein (Bang *et al.*, 2002). An anomaly of the desmin–nebulette interaction caused by a glutamic to aspartic acid mutation in desmin at position 245 underlies a human desminopathy (Vrabie *et al.*, 2005; Strach *et al.*, 2008; Conover *et al.*, 2009). Desminopathies belong to a heterogeneous genetic disease entity, termed myofibrillar myopathies (MFMs), which are caused by at least 40 distinct desmin mutations and are characterized by the formation of desmin aggregates in striated muscle (van Spaendonck-Zwarts *et al.*, 2011; Claeys and Fardeau, 2013; Clemen *et al.*, 2013; Capetanaki *et al.*, 2015).

This article was published online ahead of print in MBoC in Press (http://www.molbiolcell.org/cgi/doi/10.1091/mbc.E16-04-0237) on October 12, 2016.

†These authors contributed equally to this study.

*Address correspondence to: Gloria M. Conover (gconover@tamu.edu).

Abbreviations used: ANOVA, analysis of variance; BSA, bovine serum albumin; CBB, Coomassie brilliant blue; DAPI, 4′, 6-diamidino-2-phenylindole, dihydrochloride; DIF, desmin intermediate filaments; DTT, dithiothreitol; EDTA, ethylenediaminetetraacetic acid; EGTA, ethylene glycol-bis(β-aminoethyl ether)-*N*,*N*,*N*′,*N*′-tetraacetic acid; ELISA, enzyme-linked immunoabsorbent assay; EM, electron microscopy; GAPDH, glyceraldehyde 3-phosphate dehydrogenase; GSD, ground-state depletion; His, histidine; IF, intermediate filament; IgA, immunoglobulin A; IgG, immunoglobulin G; MFM, myofibrillar myopathy; ON, overnight; PBS, phosphate-buffered saline; PMSF, phenylmethylsulfonyl fluoride; RD, rhabdomyosarcoma; RT, room temperature; ULF, unit-length filament; WT, wild type.

Myofibers are made of serially connected sarcomeres that consist of remarkably near-crystalline highly uniform filamentous arrays. Desmin IFs (DIFs) attach to myofibers mainly at the Z-disks, that is, transversally, and intercalated disks in the case of cardiomyocytes, but also extend along sarcomeres, that is, longitudinally (Granger and Lazarides, 1978; Wang and Ramirez-Mitchell, 1983). Desmin, like all members of the IF protein family, has a central α-helical rod domain that is flanked by non–α-helical head and tail domains. The ability of IFs to assemble into highly ordered structures is thought to depend on the interaction of alternating clusters of acidic and basic amino acids present throughout the α-helical rod with the basic amino-terminal head domain (Koster *et al.*, 2015). Heptad repeats represent a characteristic motif of hydrophobic residues in position one and four of a seven amino acid stretch within a α-helical segment and are required for coiled-coil dimer formation. Most of the α-helical rod of IF proteins harbor heptad repeats in addition to hendecad repeats that mediate the formation of paired bundles, i.e. parallel α-helices (Chernyatina *et al.*, 2015; Koster *et al.*, 2015). Given the broad expression of IF proteins and the diverse distribution of IF proteins in the body, it has been proposed that their tissue-specialized functions may result from their interaction with tissue-specific binding partners (Herrmann and Aebi, 2004; Capetanaki *et al.*, 2015; Kornreich *et al.*, 2015; Koster *et al.*, 2015).

Nebulette belongs to the nebulin family of actin-binding proteins and thereby connects thin filaments to the Z-disks. Comparison of the nebulin and nebulette domain organization reveals that although they have a similar layout of their amino- and carboxyl-terminal ends, they differ substantially in the number of central repeats and in their tertiary organization (Pappas *et al.*, 2011; Bang and Chen, 2015). Another major difference is the absence of nebulin superrepeats in nebulette (Moncman and Wang, 2000). On the other hand, the highest degree of homology (60–85%) of nebulette to nebulin is in its 23 central 35-residue nebulin-like single modules (Moncman and Wang, 1995). Besides playing important roles early in cardiac development, nebulette, like nebulin, binds and stabilizes actin filaments (Jin and Wang, 1991; Moncman and Wang, 1999; Ogut *et al.*, 2003; Esham *et al.*, 2007). Coincidentally, abnormally short actin filaments are prevalent in ex vivo cardiomyocytes overexpressing the nebulette serine-rich and SH3 domain or the mutant desmin E245D and in skeletal muscles from nebulin knockout mice (Li *et al.*, 2004; Bang *et al.*, 2006; Conover *et al.*, 2009). While nebulette may have a more direct role than nebulin during chronic cardiac stress, both proteins in mice are important for Z-line width and Z-disk alignment (Yamamoto *et al.*, 2013; Mastrototaro *et al.*, 2015). These and other studies strongly support the idea that nebulette and nebulin function as an important structural backup that coordinates actin filament dynamics in myocytes.

The importance of nebulette and nebulin is highlighted by mutations linked to muscle disease. At least 20 distinct mutations in nebulette located in nebulin-like repeats are either causative or associated with hypertrophic cardiomyopathy and left ventricular noncompaction cardiomyopathy and with thin-wall dilated cardiomyopathy and endocardial fibroelastosis in adults and young children (Arimura *et al.*, 2000; Purevjav *et al.*, 2010; Maiellaro-Rafferty *et al.*, 2013; Perrot *et al.*, 2016). A striking correlation between nebulette and desmin was found in a heart biopsy specimen of an infant girl carrying a Q128R nebulette missense mutation. In the myofibrils of her heart, an irregular localization pattern for nebulette correlated to a notably decreased desmin Z-line localization. Interestingly, this nebulette mutation maps in the actin-binding region of nebulette within its N-terminal modules 2–3 (Purevjav *et al.*, 2010). Although the role of the N-terminal end of nebulette in the context of myofibril organization is less understood, the overexpression of nebulette's central modules 10–14 and 15–19 dramatically perturbs the distribution of tropomyosin, a thin-filament protein modulating calcium-mediated contractility (Bonzo *et al.*, 2008; Holmes and Moncman, 2008).

IFs are key cytoskeletal proteins that affect human health; hundreds of mutations in the 70 human IF genes underlie the molecular basis for at least 80 pathologies (Omary, 2009). In muscle tissues, desmin mutations are associated with all cardiomyopathy types, accompanied by progressive skeletal muscle dystrophy, neuropathy, conduction blocks, and accumulation of cytosolic protein aggregates. Although mitochondrial defects seem to play a major role in the desmin knockout mouse model (Milner *et al.*, 2000) and in a number of MFM (Jackson *et al.*, 2015), the molecular mechanisms responsible for desminopathy are still unclear. Past studies have proposed that nebulin serves as a direct link between IFs and sarcomeres by binding at multiple sites on desmin (Bang *et al.*, 2002; Conover *et al.*, 2009; Conover and Gregorio, 2011; Tonino *et al.*, 2010). More recently, some of the phenotypes associated with a gain-of-function mutation (E245D) occur in patients because of the disturbed assembly kinetics of the desmin–nebulette complex (Baker *et al.*, 2013).

The severe disruption of the desmin cytoskeleton in the hearts of children with the Q128R mutation in nebulette led us to explore an idea. We investigated the possibility that the similar domain layout of nebulin and nebulette and their shared roles in mechanosensing and force generation and transmission may be related by a shared direct interaction with the IF cytoskeleton. Of note, both nebulette and desmin are expressed at high levels at early stages during cardiac development (Holtzer *et al.*, 1982; Esham *et al.*, 2007). We hypothesized that the cardiac-specific protein nebulette, besides interacting with several sarcomeric proteins, would bind desmin directly and, furthermore, that binding of nebulette would affect the assembly of desmin filaments in vitro. Although it was previously inferred that nebulette may bind to desmin (Wang *et al.*, 2002), no biochemical evidence has been shown. Moreover, it is not known whether nebulette impacts desmin assembly. By dissecting the kinetics of the desmin–nebulette interaction in a reconstitution in vitro assay, our study elucidates novel molecular mechanisms responsible for desminopathy caused by desmin mutations without obvious assembly defects. Elevated levels of actin in our analyses of $Des^{-/-}$ mouse hearts support a model specifying a highly coordinated and cooperative relationship of nebulette and desmin toward sarcomeric actin. Altogether we show that nebulette specifically binds to desmin primarily through desmin's rod domain and that nebulette is part of a biomechanical complex involving sarcomeric actin that links myofibers to the IF network in heart muscle.

RESULTS

Nebulette a new binding partner for desmin in cardiomyocytes

Here we sought to determine whether nebulette, a protein primarily expressed in cardiac muscle, like nebulin, predominantly expressed in skeletal muscle, binds to the IF muscle protein desmin. A homology search revealed that three regions within nebulette display a high degree of residue similarity to nebulin's C-terminal modules (Supplemental Figure 1). Because nebulette's region 1 coincides with a known high-affinity desmin-binding region of nebulin modules 160–164 (Baker *et al.*, 2013), this study focused on that fragment, and a custom polyclonal antibody was made against nebulette module 4 to investigate whether desmin binds to nebulette.

To investigate whether nebulette and desmin form a molecular complex in cells, we performed three types of coimmunoprecipitation experiments. The first experiment used ex vivo chick

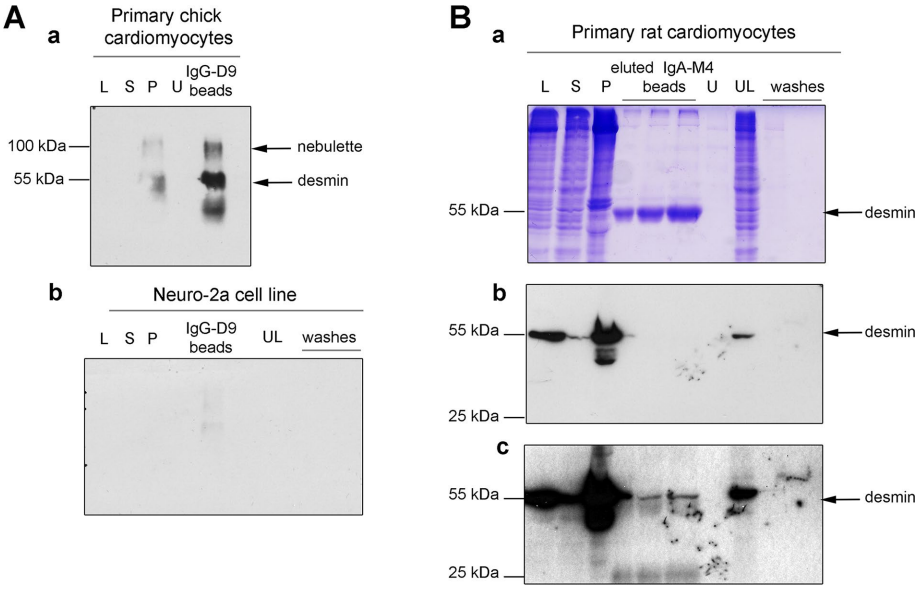

FIGURE 1: Molecular complex of desmin–nebulette in cells. (A) Small amounts of endogenous soluble nebulette (~100 kDa) were coimmunoprecipitated using protein G-agarose beads coincubated with anti-desmin D79 antibodies from the soluble lysates of ex vivo chick cardiomyocytes (Aa). The identity of nebulette was verified by Western blot using anti-nebulette M5 antibodies. In stark contrast, no nebulette bands were detected in neuro-2A lysates (Ab). (B) Magnetic IgA Dynabeads coupled to M4 nebulette antibodies were used to pull down interacting proteins in coimmunoprecipitation experiments using ex vivo rat cardiomyocyte soluble fractions. Single bands eluted from IgA-M4 beads, in the middle lanes of a CBB-stained SDS–PAGE in which the beads were loaded at three different concentrations, run below 55 kDa, which corresponds to the molecular weight of endogenous desmin (Ba). The identity of endogenous desmin in the desmin–nebulette complex detected in cardiomyocytes was verified by Western blot using anti-desmin D9 antibodies (Bb). Top blot shows a 1 min film exposure, and the bottom one shows a 5 min exposure. L, lysate; S, supernatant; P, pellet; B, beads; U, unbound proteins after Dynabeads conjugation; UL, proteins left in cell lysates after incubation with beads.

cardiomyocyte and neuroblastoma mouse cell line neuro-2A soluble-protein lysates solubilized with 50 mM Tris-HCl (pH 7.5), 150 mM NaCl, 1% NP-40, 0.5% sodium deoxycholate, and 1 mM phenylmethylsulfonyl fluoride (PMSF) spiked with protease inhibitor cocktail. Soluble lysates were incubated with G-agarose and 2 µg/ml of D76 ascites anti-desmin antibodies overnight (ON). Western blots of the immunoprecipitated beads probed with anti-nebulette M4 antibodies showed that nebulette and desmin co-precipitated only in the chick cardiomyocyte lysates (Figure 1A, compare blot Aa with blot Ab). These antibodies were made against human nebulette isoform X4 (XP_005252401) amino acids 162–181, in a region predicted to have the low cross-reactivity to nebulin (Supplemental Figures 1 and 2).

The second experiment used rat cardiomyocyte soluble-protein lysates probed with magnetic Dynabeads noncovalently bound to nebulette M4 polyclonal antibodies (Figure 1, Ba). Again, most of desmin remained insoluble in the pellet, leaving a small amount of soluble protein available for testing in coimmunoprecipitation assays. Nevertheless, endogenous soluble desmin was recovered in the eluted Dynabead immunoglobulin A (IgA)-M4 beads, indicating that nebulette binds to desmin in cardiomyocytes. The identity of desmin within the immunoprecipitated complex was confirmed by Western blot (Figure 1B).

The third experiment used a rhabdomyosarcoma (RD) cell line derived from human skeletal muscle transiently expressing pIRES His-nebulette M1–5. Although most of desmin and His-tagged nebulette remained in the pellet, and the transiently expressed nebulette was undetected by Western blot, endogenous desmin was detected in the bead sample. In contrast, no desmin was immunoprecipitated in lysates derived from vimentin$^{-/-}$ fibroblast cell line lysate, presumably because no IF proteins (desmin or vimentin) were present, suggesting that it was likely not a non-specific interaction with desmin that occurred in RD cells overexpressing nebulette (Supplemental Figure 2). Collectively the evidence indicates that nebulette and desmin likely form a molecular complex in cells.

Binding activity of desmin to nebulette primarily involves the α-helical rod

To characterize how nebulette binds to desmin in vitro, we used a biochemical approach, an IF assembly cosedimentation assay. Ionic strength and pH are the major determinants for IF assembly in vitro (Herrmann *et al.*, 2004). This assay was previously used to study the binding kinetics of nebulin to desmin during IF assembly (Baker *et al.*, 2013). Here a recombinant nebulette protein encompassing modules 1–5 was expressed, affinity purified, and centrifuged at high speed to ensure that the sample mostly was soluble nebulette (Supplemental Figure 3). For determining whether nebulette binds to desmin tetramers, the smallest soluble complex stable under low-salt conditions (5 mM Tris-HCl, pH 8.4, 1 mM ethylenediaminetetraacetic acid [EDTA], 0.1 mM ethylene glycol-bis(β-aminoethyl ether)-*N*,*N*,*N*′,*N*′-tetraacetic acid [EGTA], and 1 mM dithiothreitol [DTT]), desmin tetramers were placed on 10–70% sucrose gradients and ultracentrifuged for 5 h. Immunoblots of proteins separated by conventional SDS–PAGE showed that the majority of the desmin oligomer complexes alone were recovered in fractions 1–3 (Figure 2A). Under the same buffer conditions, nebulette M1–5 was recovered on the top fraction 0 (Figure 2B). This shows that, by itself, each protein alone forms a low molecular weight complex. However, when nebulette was coincubated with desmin tetramers before centrifugation, both proteins were completely found in the low (11 and the pellet) fractions. This points to the formation of high-molecular-weight complexes between desmin and nebulette (Figure 2C).

To determine which desmin domain is most important for nebulette binding, we tested several domain-truncated desmin variants in cosedimentation assays (Figure 3; unpublished data). Like WT desmin, the desmin rod is soluble under the same assembly conditions described above (compare amounts of rod in supernatant with pellet in Figure 3B). In contrast, when desmin and nebulette are coincubated they sediment in a complex (Figure 3A, lane P, and 3B, lane 9). These analyses suggest that the rod domain of desmin likely harbors more than one high-affinity binding site for nebulette. For the soluble desmin rod to form higher molecular weight complexes with nebulette, both proteins likely harbor multiple binding sites; otherwise, only tetrameric desmin–nebulette complexes would be expected to form. Sedimentation of protein complexes to the

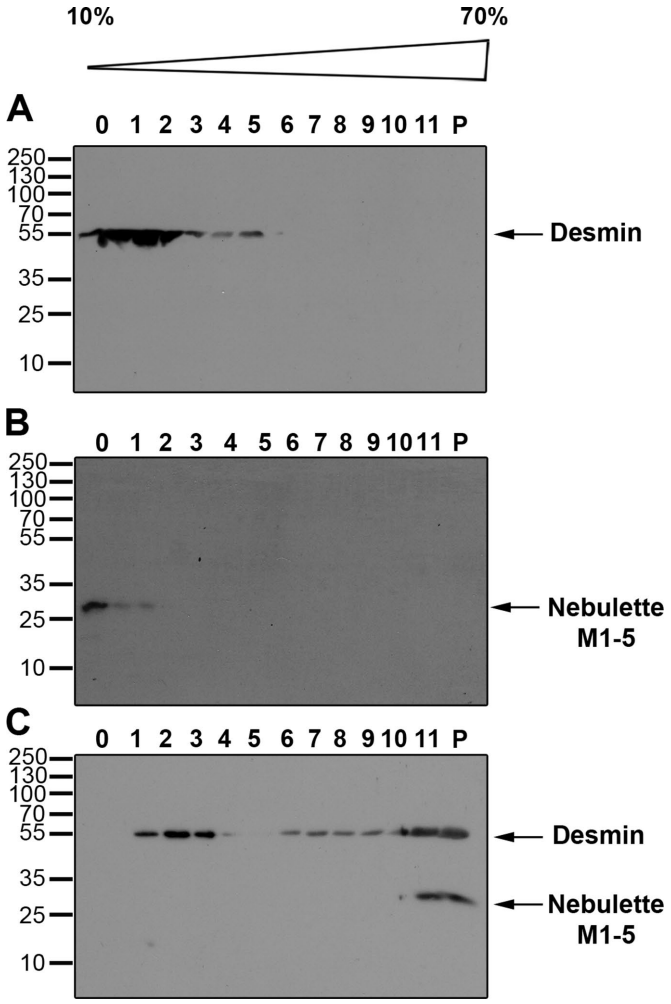

FIGURE 2: Direct protein–protein interaction of nebulette and full-length desmin. A specific biochemical interaction of nebulette to desmin was detected under buffer conditions that restrict desmin filament maturation by sucrose gradient sedimentation. Soluble desmin oligomers and nebulette M1–5 recombinant proteins were precleared from small aggregates by ultracentrifugation. Desmin alone (A) or nebulette alone (B) or in a 1:1 M ratio mixture (C) were incubated for 1 h at 37°C and placed on top of 10–70% sucrose gradients made in a buffer (5 mM Tris-HCl, 1 mM EDTA, and 0.1 mM EGTA, pH 8.4) that favors desmin oligomer formation. After a 5 h sedimentation at 42,000 rpm, fractions (1–10 and pellet) were collected and analyzed by 12% SDS–PAGE and Western blot. Arrows point to bands for desmin or nebulette M1–5, migrating at their expected molecular weights of 52 and 25 kDa, respectively.

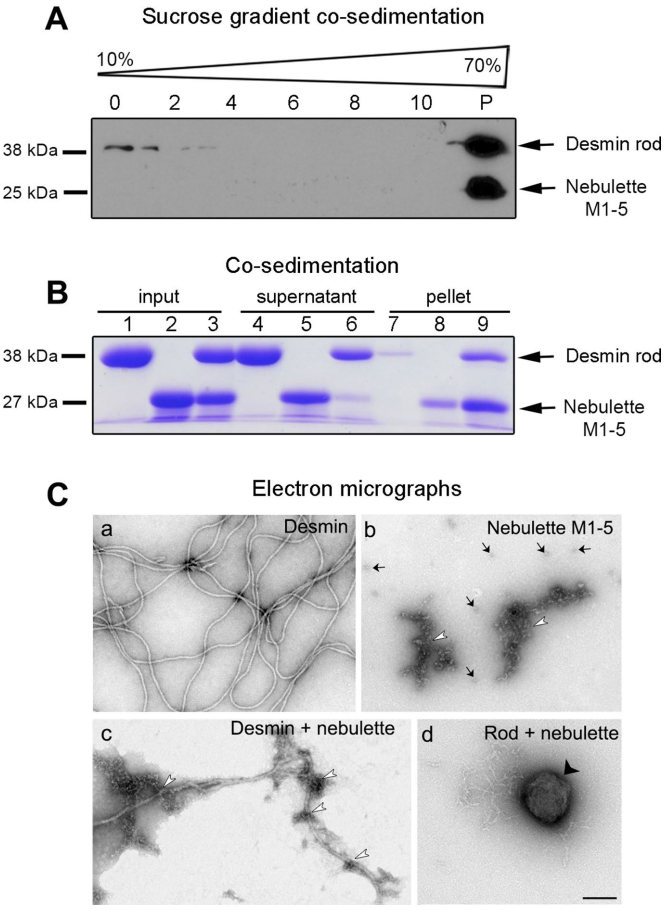

FIGURE 3: Nebulette binds to desmin primarily by its α-helical rod domain. (A) Western blot detecting desmin rod and nebulette M1–5 proteins compares sedimentation profiles in a sucrose gradient sedimentations experiments mixing nebulette M1–5 with desmin rod. All the proteins used in these cosedimentation assays were centrifuged in an airfuge for 30 min at 30 psi before incubation for 1 h at 37°C in 5 mM Tris, 1 mM EDTA, 0.1 mM EGTA, and 1 mM DTT (pH 8.4). (B) CBB-stained gel lanes: human desmin rod (lanes 1, 4, and 7); nebulette M1–5 (lanes 2, 5, and 8), 1:1 M ratio of desmin rod and nebulette (lanes 3, 6, and 9). (C) Desmin filaments bound or not to nebulette were visualized by EM. Proteins were coassembled for 30 min at 37°C before being deposited on grids. The ultrastructure of nebulette oligomers (arrows) and larger clusters (arrowheads) were visualized in a grid containing only nebulette (Cb). A direct association of nebulette along bent WT desmin filaments (Cc). Desmin rod protein mixed in 1:1 M ratio with nebulette forms 3–4 μm rounded structures (Cd). Scale bar: 200 nm.

low-sucrose fractions was also obtained in experiments testing for nebulette binding to headless or tailless desmin (unpublished data), thus indicating that neither the head nor the tail of desmin alone are sufficient to prevent the desmin–nebulette complex from forming. Collectively these data demonstrate that nebulette and desmin form a specific molecular complex in vitro. Furthermore, we predict that the nebulette M1–5 segment alone is capable of cross-linking DIFs.

Ultrastructure of desmin filaments bound to nebulette

To study how nebulette may structurally influence desmin during its in vitro assembly, we evaluated desmin–nebulette complexes using EM. Unlike microfilaments and microtubules, IFs do not require ATP or GTP to form filaments and networks from monomers. A shift to a higher ionic strength causes desmin oligomers to assemble into filaments (see *Materials and Methods* for more details). Smooth naked desmin filaments were visualized 30 min after assembly was initiated (Figure 3Ca). Conversely, the nebulette M1–5 protein had a grape-like appearance, either as small oligomers or larger clusters (Figure 3Cb, compare arrows with arrowheads). These nebulette structures resemble those previously reported for nebulette fragment C5N (Cherepanova *et al.*, 2006) and are also very similar to nebulin structures binding desmin or bundling actin filaments (Gonsior *et al.*, 1998; Baker *et al.*, 2013). When desmin oligomers and nebulette were coincubated under buffer conditions that favor desmin filament assembly, an intimate association was revealed (Figure 3Cc). Desmin filaments appeared to be covered by intermittent nebulette patches.

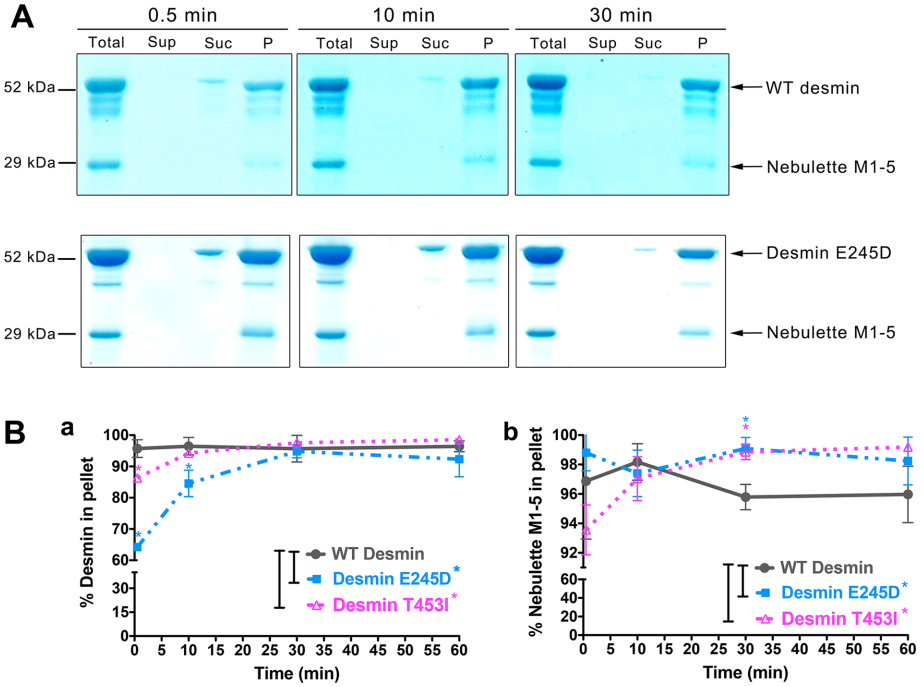

FIGURE 4: Differential binding kinetics of mutant desmins to nebulette. The binding of nebulette M1–5 to two filament-forming mutant desmins linked to desminopathy was tested during time-dependent assembly in cosedimentation assays. (A) Representative CBB-stained SDS–PAGE gels show total, supernatant (Sup), sucrose cushion (Suc), and pellet (P) fractions for equimolar mixtures nebulette M1–5 with either WT desmin (top gels) or desmin E245D (bottom gels). (B) Changes in the assembly kinetics of WT and mutant desmin in the presence of nebulette. The densitometry values were quantified for each protein at discrete time intervals for 1 h at 37°C. The percentage of protein obtained in the pellet is plotted based on the total amount of protein used at the beginning of the assay. The data show that mutant desmin E245D displayed delayed binding to nebulette, compared with WT desmin, during the first 15 min of assembly, while slower kinetics was found for mutant desmin T453I during the first 7 min of assembly (Ba). Lower amounts of nebulette were recovered in the pellets for WT after 30 min of assembly compared with the mutant desmins (Bb). Mean ± SD for each time point is plotted as determined from band densitometry measurements in three experiments. Significance was determined using Student's *t* test comparing full-length WT desmin to mutant desmin (*, $p < 0.05$).

In contrast, large round structures with diameters ranging from 0.1 to 0.3 μm readily formed when nebulette M1–5 and desmin rod were mixed (Figure 3Cd). On the basis of these observations, we speculate that nebulette, like nebulin in myocytes, has the capacity to set the direction of the desmin filaments by binding to particular pressure points on their multiple binding sites on the desmin network.

Delayed binding of nebulette to mature filaments assembled from mutant desmins

Myofibrils must perfectly align and realign to produce and transmit force effectively. Thus defects in sarcomere–IF network connectivity may result in sarcomere malfunction and eventually cause disease. Hence we examined whether the binding activity of nebulette to desmin was affected by the mutations E245D and T453I in desmin that cause desminopathies, although in vitro they assemble into seemingly normal filaments (Bar *et al.*, 2005). We tested these two desmin missense mutants for binding to nebulette in filament assembly buffer (25 mM Tris-HCl, 50 mM NaCl, pH 7.5) and followed the amount of protein sedimentation by SDS–PAGE. We found that both mutants were delayed in binding nebulette compared with wild-type (WT) desmin, as shown here for desmin E245D (Figure 4A). The densitometry analysis of three independent sedimentation runs demonstrated that, during the first 10 min of desmin assembly, mutant desmin E245D was significantly slower than WT desmin, and during the first 3 min, mutant desmin T453I was significantly slower than WT desmin (Figure 4B). Moreover, the network formation was complete by 30 min, since at 60 min practically the same values were obtained for the percentage of protein found in the pellet. Hence these results demonstrate a clear difference in the physical interaction of the mutants with nebulette compared with WT desmin that may be important in a physiological setting.

Nebulette binds mutant desmins with increased binding affinity

To determine the binding affinity of nebulette to desmin in vitro, we used an enzyme-linked immunoabsorbent assay (ELISA). Purified nebulette was absorbed onto microtiter plates and incubated with increasing amounts of full-length desmin tetramers. These experiments revealed that desmin binds strongly to nebulette N-M6 or M1–5 fragments with a high-affinity saturable binding (K_d = 12–19 nM, Figure 5A). Interestingly, the range for these binding affinities closely agrees with the range reported for desmin and nebulin modules 160–164 (K_d = 10–18 nM; Baker *et al.*, 2013).

Previous reports suggested that the timing and strength of desmin E245D binding to nebulin is abnormal (Conover *et al.*, 2009; Baker *et al.*, 2013). Given that we found a high specific interaction between desmin and nebulette, we wondered whether mutant desmin E245D and T453I may have altered binding affinities to nebulette. Incidentally, both of these desmin mutations locate within reported nebulin-binding desmin peptides (Conover and Gregorio, 2011). We found that both mutations had a consistently enhanced binding affinity to nebulette, with an estimated K_d of 5–6 nM and 3 nM, respectively (Figure 5, B and C). Both mutants exhibited significantly increased binding capacity. Therefore our results suggest that tighter protein–protein interactions between desmin and nebulette may alter the connectivity of sarcomeres to the IF cytoskeleton.

Nebulette fluidizes heterogeneous mutant desmin networks

The viscous behavior of the IF network most likely impacts all intracellular processes in cardiomyocytes, including their beating activity. Initially, we compared the network viscosity profiles formed by WT and mutant desmin for 30 min. We show that, under the conditions tested, WT desmin formed networks quickly, within the first 3 min of assembly. This behavior is different from networks made from mutant desmin E245D, which formed three to four times more slowly, indicating that mutant desmin makes a more fluid IF network (Figure 6, compare black with red profile). The assembly rate of an equimolar mixture of WT and mutant desmin E245D plateaus very rapidly, within the first seconds of assembly, indicating that this protein mixture forms extremely viscous IF networks (Figure 6, compare black with dark green profile).

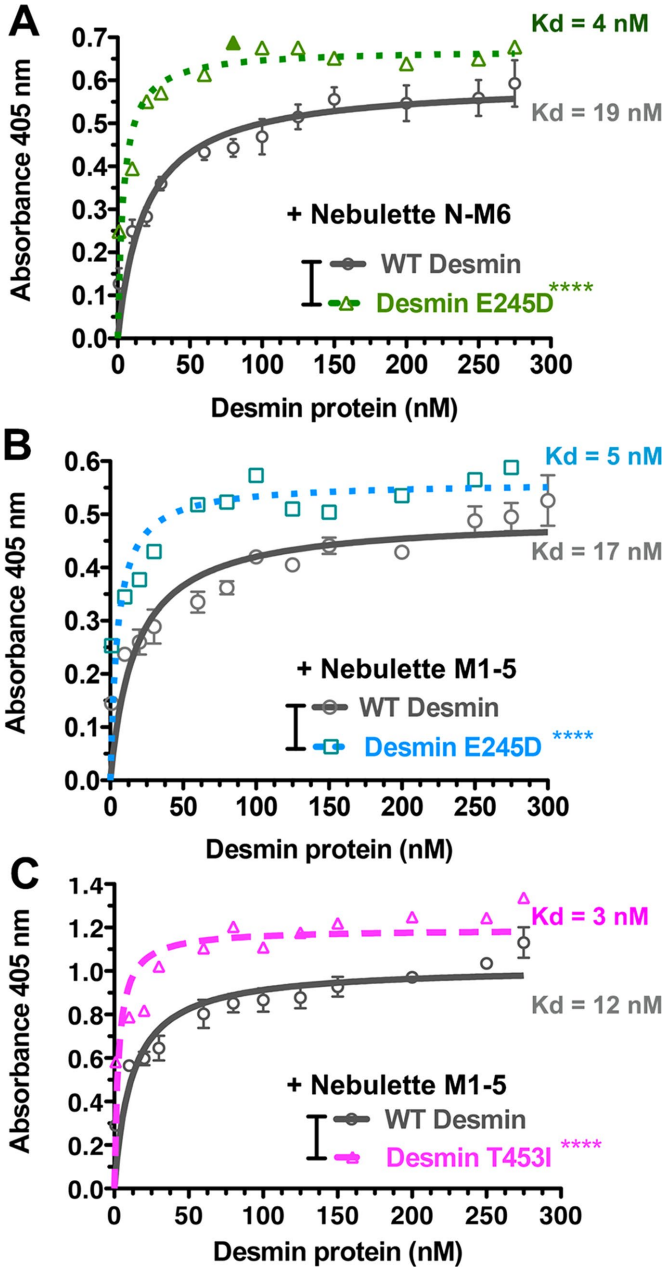

FIGURE 5: Mutant desmin has increased binding affinity to the N-terminal nebulette. A specific interaction between recombinant full-length desmin in solution and nebulette M1–5 proteins seeded on triplicate wells on microtiter plates was detected through ELISAs. (A–C) Graphs show a nonlinear fit curve that estimates a dissociation constant (K_d) for the WT desmin and nebulette M1–5 interaction of 16–24 nM. Our data consistently showed higher affinity binding when nebulette N-M6 (A) or M1–5 (B and C) fragments were tested for binding to desminopathy-linked mutant desmin E245D (A and B) or mutant desmin T453I (C). The estimated K_d for mutant desmin bound to nebulette was ~5 nM. This elevated specific binding was accompanied by a reproducible increase in binding capacity (B_{max}) in mutant desmin relative to WT desmin. A representative assay was selected from two to five independent experiments. Significance was determined using Student's *t* test comparing full-length desmin pellet sedimentation with the mutant variants in triplicate wells per each time point (****, $p < 0.0001$).

To address whether nebulette impacts desmin network assembly, we added nebulette M1–5 to excess amounts of WT desmin or to the mutant desmins. We showed a slower increase in the viscosity for the WT desmin network in the presence of nebulette than without it, suggesting that nebulette binding opens up the DIF network (Figure 6Aa, compare gray with black profile). On the contrary, when nebulette was added to mutant desmin E245D, the viscosity of the mutant network increased, suggesting that nebulette binding stiffens the homozygous mutant network (Figure 6Bb, compare pink with red profile). A more pronounced decrease in viscosity was observed when nebulette was added to a heterozygous equimolar mixture of WT and mutant desmin (Figure 6Ca).

Visualization of all three IF networks coincubated with nebulette by EM revealed some clues about why nebulette binding increases the mutant viscosity when it decreases WT and heterozygous desmin network viscosity. Comparison of grid areas suggests that more nebulette oligomers seemed to attach to mutant desmin E245D than to WT desmin. Images show a more open fluid conformation for WT desmin networks than for the stickier mutant desmin networks binding nebulette (Figure 6, compare arrows in Ab to arrows in Bb). On the other hand, larger voids were noticeable in heterozygous networks, possibly because spacing irregularities in the binding sites for nebulette on the heterozygous networks enable promiscuous cross-links (Figure 6, compare Ab with Cb). These results demonstrate that nebulette binding changes the viscosity of IF desmin networks and suggest that the binding of nebulette to desmin may dictate to some extent the slack of the DIF networks in cardiomyocytes.

Nebulette module 4 circumscribes desmin filaments

To achieve a high-resolution image of the desmin–nebulette complex in ex vivo chick cardiomyocytes and define the localization of the nebulette module 4, we imaged cells in parallel by wide-field superresolution ground-state depletion microscopy (GSD). GSD improves the resolution through forcing neighboring fluorophores to separate by turning most of them dark with a high-powered emission laser. An image was reconstructed in real time by registering the position of the fluorophores that did not turn dark and by adding the high-precision positions of the dark fluorophores when they returned to the ground state. In this way, we resolved individual sarcomeres in a 20 × 20 μm box in fixed cells stained for tropomyosin, an integral component of actin filaments (Supplemental Figure 4A).

A terrific localization for nebulette module 4 that closely followed the honeycomb-like pattern observed for the desmin network was obtained using GSD (Figure 7A and Supplemental Figure 4Bh). Even though the nebulette signal was in close proximity to the desmin signal (see arrowheads in Figure 7Ab), the nebulette module 4 did not overlap completely with desmin in all planes imaged, suggesting that the N-terminal module M4 of nebulette extends out from the I-Z-I bands. The subcellular localization of desmin observed in these cells is highly reminiscent of the in-register Z-disks connected by desmin-containing, honeycomb-like IF arrays, originally described for isolated myofibril Z-disks from chicken muscle (Granger and Lazarides, 1979). This technique allowed us to visualize an elaborate subcellular geometry of desmin and nebulette networks intertwined at the Z-disks at high resolution.

The subcellular localization of nebulette module 4 in cardiac striated muscle was investigated further by spectral confocal *z*-planes of mammalian tissue samples (Figure 7B). In rat hearts, nebulette module 4 is easily distinguished in the form of doublets and has a clear desmin striation in the middle (see arrowheads in Figure 7Ba). At a high magnification, a three-dimensional view shows that

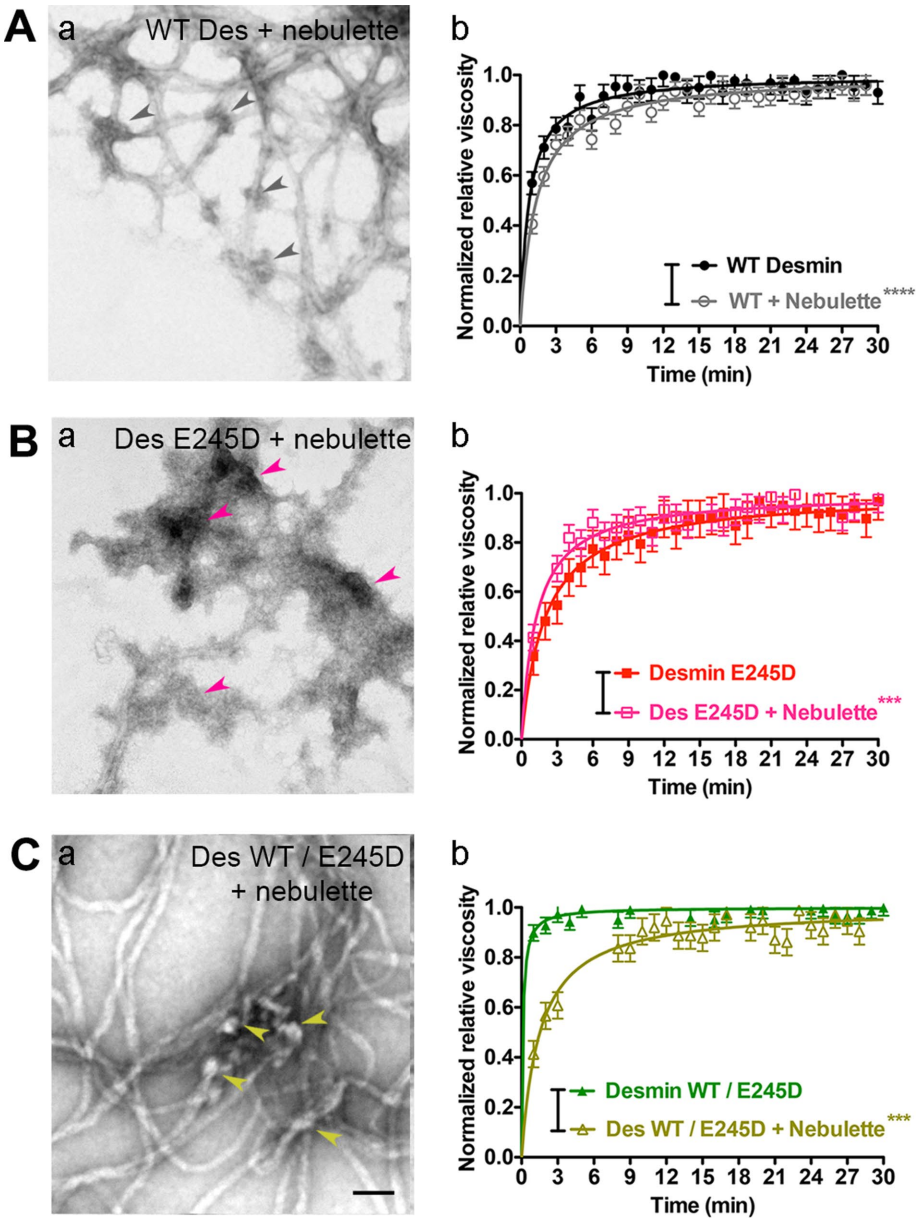

FIGURE 6: Nebulette fluidizes desmin networks early during assembly. The impact of nebulette binding on desmin assembly kinetics was determined by measuring changes of the IF network viscosity in WT desmin (Aa), mutant desmin E245D (Ba), and heterozygous WT and mutant desmin (Ca) networks. The relative viscosity measured at 37°C was plotted as the averaged normalized data for a 30 min reaction. The linear fits of normalized data ± SD were as follows: for WT desmin, $n = 4$ (K_d range: 0.657–0.866); for desmin E245D, $n = 4$ (K_d range: 1.889–2.888); for Des WT/ Des E245D, $n = 3$ (K_d range: 0.0597–0.1619); and for WT desmin plus nebulette, $n = 3$ (K_d range: 1.234–1.491). The errors for desmin E245D plus nebulette and Des WT/ Des E245D plus nebulette were estimated from the variance of these samples without nebulette. These were for desmin E245D plus nebulette, $n = 1$ (estimated K_d range: 1.118–1.429), and for Des WT/ Des E245D plus nebulette, $n = 1$ (estimated K_d range: 1.285–1.751), given that only one experiment was available. Significance between samples was determined using a paired Student's t test (***, $p < 0.01$; ****, $p < 0.0001$). Visualization of the DIF network ultrastructure with or without nebulette. Electron micrographs show nebulette binding opens the WT desmin networks (Ab), while a stickier nebulette closes the mutant E245D networks (Bb). Arrowheads point to areas of higher avidity of nebulette to mutant desmin E245D compared with WT desmin (compare Bb with Ab). Large clumps of nebulette accumulate in the areas where the mutant filament bends. In contrast, WT / E245D networks (1:1 M ratio) creates promiscuous nebulette cross-links on uneven heterozygous networks (Cb).

nebulette appears to surround desmin, which, at the angle shown, can be viewed as a distinct nebulette doublet (see arrowheads in Figure 7Bd).

Lack of desmin dysregulates cardiac α-actin protein levels

Understanding the functional relationship between desmin and nebulette in heart muscle sarcomeres is an important step in discerning its role in familial cardiomyopathies (Purevjav *et al.*, 2010). To gain a better insight into the relationship of desmin and nebulette with sarcomeric actin, we used the Des$^{-/-}$ mouse knockout model, previously reported to have elevated levels of skeletal α-actin and without indication of catastrophic structural defects (Milner *et al.*, 1996). To test our hypothesis that nebulette is the link between desmin and actin, in this study, we inquired whether cardiac α-actin was dysregulated in the Des$^{-/-}$ heart myofibers (Figure 8A). We propose that nebulette is a good candidate for a cross-linker protein, given that many reports implicate it as a primary stabilizer of cardiac actin filaments (Moncman and Wang, 1999; Kazmierski *et al.*, 2003; Bonzo *et al.*, 2008; Littlefield and Fowler, 2008). We quantified the total α-actin protein levels in WT and Des$^{-/-}$ Sv129 mice hearts by Western blot using two different actin antibodies (for details, see *Materials and Methods*). Band densitometry values were normalized relative to the total content of glyceraldehyde 3-phosphate dehydrogenase (GAPDH), and their relative levels were quantified. The level of cardiac actin was elevated up to four times in Des$^{-/-}$ hearts compared with WT controls (19 ± 3 for WT compared with 68 ± 6 in Des$^{-/-}$ hearts; Figure 8B). A more pronounced difference in the levels of α-sarcomeric cardiac actin was found in Des$^{-/-}$ hearts, which had up to five times higher levels than WT mice (19 ± 5 for WT compared with 87 ± 6 in Des$^{-/-}$ hearts; Figure 8C). In contrast, we found that WT mice hearts contained twice the levels of vimentin compared with Des$^{-/-}$ hearts (Figure 8C). The fact that actin levels are altered in the absence of desmin support the idea that nebulette may functionally link sarcomeric actin to the desmin cytoskeleton. Furthermore, our results give insights into the altered actin disorganization reported in cardiomyocytes overexpressing nebulette (Moncman and Wang, 2002) or mutant desmin (Conover *et al.*, 2009).

Desmin impacts nebulette organization in sarcomeres

To better define the functional relationship between desmin and nebulette in vivo, we

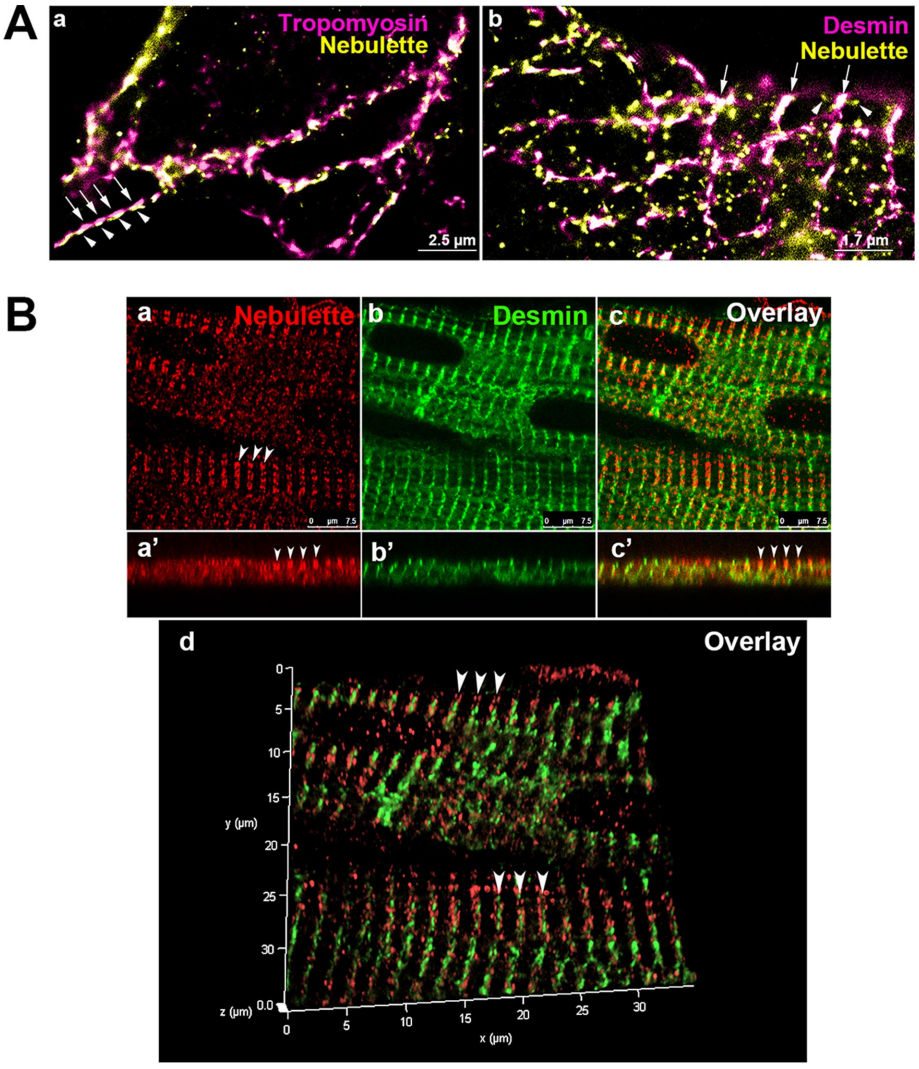

FIGURE 7: Localization of nebulette's module 4 relative to desmin in cardiac muscle. The spatial distribution of nebulette N-terminal module 4 relative to desmin was assessed in ex vivo chick cardiomyocytes and in heart paraffin sections. (A) Enlarged GSD images show cardiomyocytes stained with nebulette (yellow) and costained either for thin-filament marker tropomyosin (a, pink) or IF desmin (b, pink). Arrows in image Ab point to consecutive Z-disks heavily enriched for desmin (pink) with nebulette module 4 (yellow) emanating bidirectionally (arrowheads) from either side of desmin striation. White color indicates the areas of colocalization of desmin and nebulette module 4 in the plane imaged. (B) Nebulette's module 4 borders both sides of the Z-disk–associated desmin as detected with the M4 polyclonal peptide nebulette antibody. Confocal images of individual optical sections distinguish numerous nebulette doublets bordering desmin striations (Bc) in cells costained for nebulette and desmin using monoclonal Dako desmin antibody. Note that most of the nebulette doublets surround desmin (Bd, arrowheads). Insets show higher magnification of the nebulette doublets overlapped with desmin in side view (z-axis) and in three-dimensional graphs. Scale bar: 10 µm.

evaluated the distribution of nebulette in WT and Des$^{-/-}$ hearts by confocal microscopy. Many Des$^{-/-}$ heart myofibrils had no visible nebulette (compare z-stack views in Figure 9A). The few Des$^{-/-}$ myofibrils with well-defined sarcomeres had disorganized nebulette striations (Figure 9, Aa compared with Ad). For example, note the prevalent voids in the axial views of the Des$^{-/-}$ myofibrils with no discernible striated nebulette (Supplemental Movie).

To delineate whether changes in nebulette organization may result from the absence of desmin cytoskeleton in Des$^{-/-}$ myofibrils, we determined the gray-value intensity of nebulette along myofibrils on the same focus plane. Analyses revealed that the nebulette organization was remarkably abnormal in Des$^{-/-}$ hearts. Line profiles demonstrated that the regularly spaced striations common in WT myofibrils were, in contrast, short and flat in the Des$^{-/-}$ myofibrils (Figure 9B). In fact, lack of periodicity was quantified by comparing the Des$^{-/-}$ and WT hearts average nebulette striation separation. Data show a significant difference between WT (0.99 ± 0.12 µm, $n = 205$) and Des$^{-/-}$ myofibrils (0.92 ± 0.15 µm, $n = 205$).

To determine whether nebulette M4 sarcomere targeting depends on desmin, we analyzed the global total image intensity of nebulette M4 stain per pixel on intact myofibers. As expected, a significant difference was found in myofibers stained for desmin (Figure 9C). The average desmin intensity for WT hearts was 23.7 ± 8.5 compared with 15.3 ± 4.2 in Des$^{-/-}$ hearts. However, surprisingly, we found no significant difference in the cumulative intensity distribution for myofibers stained for nebulette M4 between WT and Des$^{-/-}$. Specifically, the mean values show that nebulette intensity in WT hearts was 12.0 ± 2.3, which is not significantly different from 13.8 ± 4.3 in Des$^{-/-}$ hearts. Thus, since the overall intensity of nebulette on sarcomeres is unchanged in Des$^{-/-}$ and WT hearts, these data indicate that desmin is not absolutely required for nebulette assembly and that other redundant proteins may substitute for desmin function when absent.

For evaluating whether desmin regulates nebulette protein levels, heart lysates from WT and Des$^{-/-}$ hearts were prepared and analyzed by Western blot (Figure 9D). Band densitometry shows an ~56% decrease in nebulette protein levels in Des$^{-/-}$ hearts relative to WT. Consistent with these results, an ~109 kDa band corresponding to full-length soluble nebulette was detected in lysates prepared from WT hearts, while it was barely detected in Des$^{-/-}$ hearts (unpublished data). Collectively we infer that desmin impacts nebulette's fine sarcomere organization on myofibrils rather than its absolute ability to target to the sarcomere. We also infer that absence of desmin decreases the total amount of nebulette in Des$^{-/-}$ hearts by altering their actin dynamics. Follow-up studies should clarify the specific effect of desmin–nebulette on dynamics of the myocyte actin cytoskeleton.

DISCUSSION

Desmin forms an intricate three-dimensional cytoskeleton that organizes myofibers within striated muscle. The mechanisms that regulate Z-disk and thin-filament stabilization and organization in sarcomeres and their interplay with the extrasarcomeric cytoskeleton remains incompletely understood. Here we show that nebulette, a protein important in myofibrillogenesis and Z-line assembly, directly

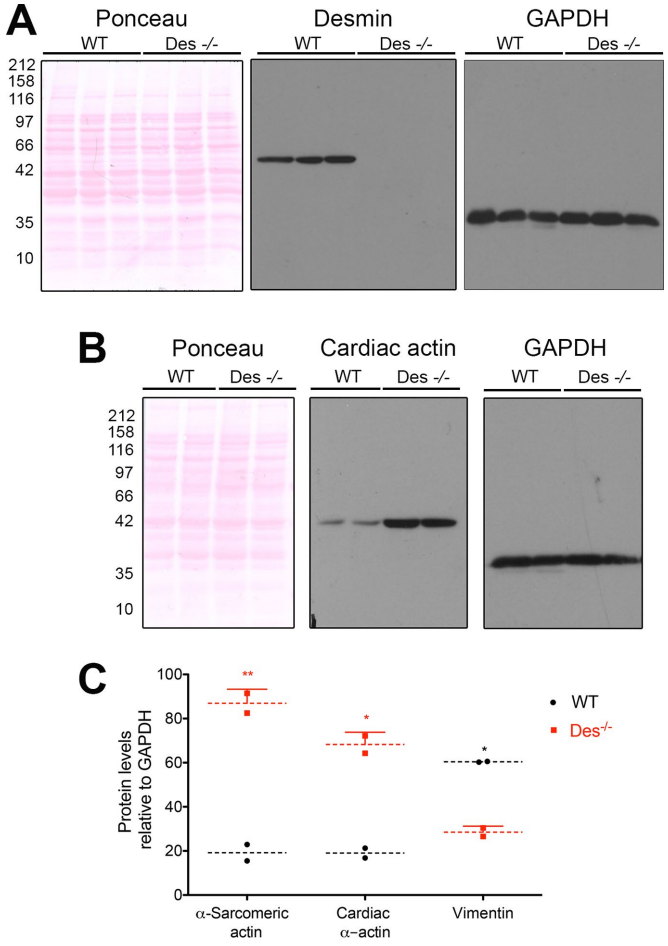

FIGURE 8: Elevated cardiac actin levels in Des$^{-/-}$ mouse hearts. (A) Panel display the total protein content in ponceau-S–stained blot runs using lysates made from homogenized whole-tissue hearts dissected from WT and Des$^{-/-}$ Sv126 strain mice ($n = 3$ per group). Western blot shows desmin migratating at 52 kDa in WT hearts while absent entirely from Des$^{-/-}$ hearts. (B) Similar amounts of lysate loading are demonstrated with ponceau-S–stained blots. The protein levels of cardiac actin are significantly increased in Des$^{-/-}$ hearts compared with WT controls ($n = 2$ per group). (C) Graph displays the relative protein levels of α-sarcomeric actin, cardiac actin, and vimentin as quantified by band densitometry using ImageJ. Individual lanes were normalized to GAPDH levels. Significance between samples was determined using two-way analysis of variance (ANOVA; **, $p < 0.01$; *, $p < 0.05$).

binds to desmin in cardiomyocytes and in vitro. This evidence extends previous findings that, in skeletal muscle, desmin forms a biomechanical Z-line complex with nebulin (Bang *et al.*, 2002; Conover *et al.*, 2009; Tonino *et al.*, 2010). Besides providing myofibrillar connectivity, the desmin–nebulette complex constitutes a highway to sarcomeric actin in the heart that may fine-tune the transmission of force between sarcomeres, which ultimately may impact heart rhythm.

Impact of nebulette binding on desmin kinetic assembly

We report a rapid desmin–nebulette interaction that begins when desmin filaments are in the unit-length filament (ULF) state and continues until filaments mature (Figure 2). In vitro IF assembly generally follows lateral association of tetramers to ULFs, a longitudinal growth phase of longitudinal annealing of ULFs, and a final radial compaction of extended filaments (Herrmann *et al.*, 1999). Additionally, we provide evidence that the α-helical–rod domain of desmin is pivotal for desmin's interaction with nebulette (Figure 3). This indicates a major binding site for nebulette on desmin resides within the core of the filament.

Using kinetic cosedimentation assays, we monitored how nebulette binding changed during filament-forming mutant desmin kinetic assembly. Our study focused on the two desmin mutations. Coil 1B mutation E245D, which is close to linker L12, an important region for assembly (Herrmann and Aebi, 2004) and which is highly conserved from shark to man (Schaffeld *et al.*, 2001; Bar *et al.*, 2004); this mutation causes restrictive cardiomyopathy with skeletal pathology (Vrabie *et al.*, 2005). Also, tail mutation T453I, which causes restrictive cardiomyopathy and atrioventricular block, hits a highly conserved amino acid in a part of the tail that may carry a functional structural motif (Schaffeld *et al.*, 2001; Arbustini *et al.*, 2006). Interestingly, we found a subtle but reproducible retardation of nebulette binding to mutant desmin (Figure 4). A sharp drop in network viscosity in heterozygous WT/E245D networks (Figure 6) suggests the delay in nebulette binding to desmin during assembly may create fluid pockets that encourage nonspecific protein–protein interactions. These desmin network perturbations probably detach sarcomeres from the plasma membrane, thereby negatively impacting heart rhythm. Future in vivo studies should address this possibility.

Mutant desmins bind nebulette tighter

ELISAs confirm that nebulette, like nebulin, has enhanced binding affinity to the filament-forming mutant desmins investigated here (Figure 5). On the basis of slow-assembly kinetics, electron micrograph observations, and viscometry assays, we predict that mutant desmin E245D and T453I likely form wider and stickier myofibers. Slower filament assembly may cause local myofibril disorganization, partially disturbing the desmin cytoskeleton in cardiomyocytes. Incidentally, a study showed other filament-forming mutant desmin had weaker strain stiffness and defective strain responses (Bar *et al.*, 2010). Thus the phenotypes we report for our mutant desmin may result from perturbations in the subunit exchange rates and abnormal mass per length ratios within filaments. The defects in mutant desmin binding to nebulette reported here should be evaluated in animal studies.

Roles of the desmin–nebulette linkage on sarcomeres

Nebulette, an actin-binding protein that interacts with tropomyosin, myopalladin, and α-actinin, stabilizes a short core of the actin filaments near the Z-disks (Littlefield and Fowler, 2008). Despite this information, it remains unclear how sarcomeres coordinate their stretch–strain cycles with desmin's well-documented role in muscle force transmission. Clues to a possible role for nebulette as a regulatory or linker protein may arise from findings that infants carrying nebulette mutations Q128R and A592E with dilated cardiomyopathy and endocardial fibroelastosis also display low desmin targeting (Purevjav *et al.*, 2010). Here we investigated how the absence of desmin affects nebulette in the myocardium of Des$^{-/-}$ knockout mice. We found abnormally high actin levels, suggesting a functional dependence among these three proteins in heart. Remarkably, Des$^{-/-}$ knockout and transgenic nebulette Q128R mice share atypical lysosomes, mitochondria, and intercalated disks (Bang and Chen, 2015; Capetanaki *et al.*, 2015). To suggest that desmin–nebulette partnership may account for some of these defects in cardiomyocytes is tempting and requires further study.

Here we report two important findings. First, actin levels are elevated in Des$^{-/-}$ hearts, and nebulette total levels are decreased.

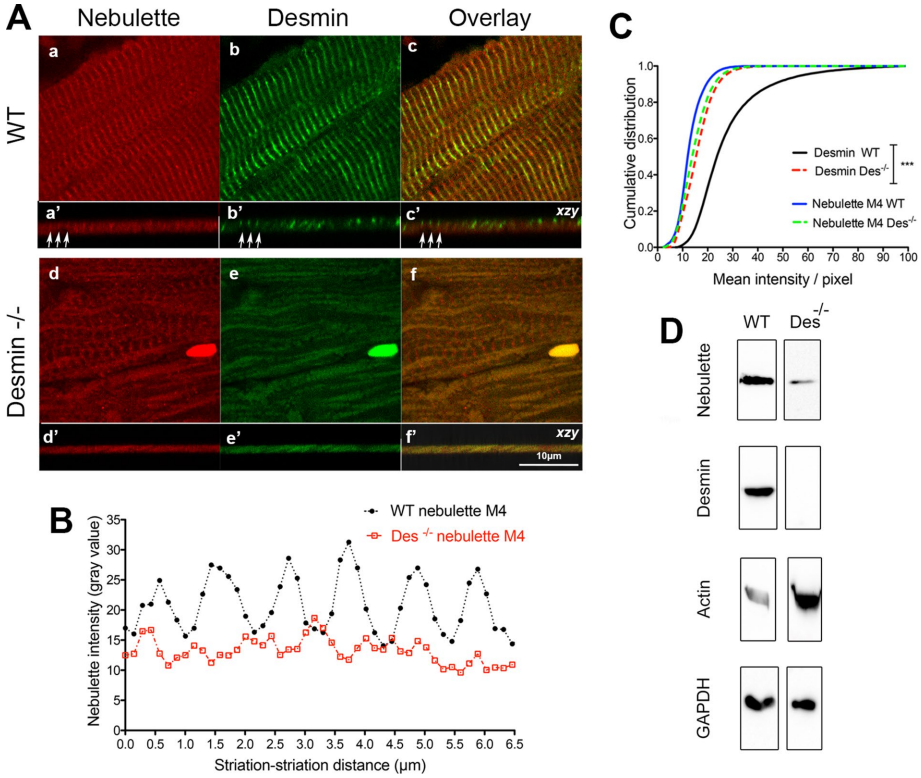

FIGURE 9: Alterations in nebulette organization and total levels in Des$^{-/-}$ hearts. Panels show confocal micrographs of paraffin-embedded hearts dissected from Sv126 strain mice costained for nebulette and desmin. (A) The majority of the myofibrils in Des$^{-/-}$ hearts do not target nebulette well, while the minority show irregularly spaced striated nebulette (compare Ad to Aa). Comparison of the three-dimensional volume side views (*z*-axis) of WT to Des$^{-/-}$ myofibrils (Aa′ to Ad′) show smooth flat myofibrils without prominent striations. (B) Line-profile plots display the nebulette intensity of individual myofibril analyzed in images from individual WT and Des$^{-/-}$myofibers. (C) Graph displays the cumulative distribution of the total nebulette mean intensity levels per pixel, determined from images costained for desmin and nebulette from samples staining WT and Des$^{-/-}$ hearts. Significance between samples was determined using two-way ANOVA (*** $p < 0.001$). (D) Western blot of whole-heart lysates compares the total protein levels of nebulette, desmin, and actin in WT and Des$^{-/-}$ samples. GAPDH was used as loading control.

Although beyond this study's scope, we speculate that the binding of nebulette to actin may be disrupted in Des$^{-/-}$ knockout hearts or in patients' hearts bearing one of the 20 nebulette mutations reported to date (Arimura *et al.*, 2000; Purevjav *et al.*, 2010; Maiellaro-Rafferty *et al.*, 2013; Perrot *et al.*, 2016). Nevertheless, our study indicates that absence of desmin affects the homeostasis of actin cytoskeleton in cardiomyocytes and that nebulette is a prime candidate to mediate such a response. Future studies should investigate how the desmin–nebulette complex is involved in the dynamics of actin in cardiomyocytes.

Second, intact myofibers of Des$^{-/-}$ hearts display irregular nebulette incorporation within their thin filaments, as evidenced by the variable spaced striations (Figure 9, A and B). Without desmin, most of the myofibrils disconnect from the extrasarcomeric cytoskeleton, which isolates the sarcomeres from the plasma membrane and the nucleus. Because the global intensity of nebulette in paraffin-embedded sections seemed unchanged between WT and Des$^{-/-}$ hearts, desmin-independent mechanisms involving other IF proteins may have redundant functions to target nebulette to the myofiber and maintain partial sarcomere function until late age-onset fibrosis develops. Vimentin, an IF structurally related to desmin, represents a good candidate to test this possibility.

A model: nebulette coordinates the functional interplay of desmin and actin

We report that desmin physically binds to nebulette in vitro and in cardiomyocytes. Des$^{-/-}$ mouse hearts have reduced nebulette and elevated actin levels, with intact myofibers showing disordered nebulette organization. The exact causes for these findings remain unknown. However, we present a model that describes our interpretation of our data, incorporates past findings, and communicates our recommendations for future studies.

Herein is our model: In healthy hearts, desmin maintains nebulette in the correct conformation to facilitate the normal cycles of actin assembly and disassembly in the sarcomere (Figure 10A). Iterative helical real-space reconstruction studies have mapped particular actin-binding sites for nebulette and nebulin repeats, suggesting that more than one nebulette molecule likely stabilizes actin (Cherepanova *et al.*, 2006). The desmin–nebulette complex stabilizes a short region of the actin filaments surrounding the Z-lines. Examination of the heart of an infant carrying a nebulette missense mutation in the region that we report here to bind to desmin revealed significant desmin disorganization (Purevjav *et al.*, 2010). Thus we think nebulette likely regulates desmin organization in cardiomyocytes spatiotemporally. Additionally, we propose that nebulette likely triggers a feedback mechanism that modulates actin levels in cooperation with desmin.

Mutant desmin binds nebulette with enhanced binding affinity, giving us reason to propose that a structural change within mutant desmin makes it bind more tightly than normal desmin to nebulette. This tighter bond retards filament elongation by trapping desmin oligomers during desmin assembly (Figure 10B). When functioning properly, desmin appears to modulate actin by ensuring that its levels are balanced in sarcomeres in collaboration with nebulette. In contrast, when desmin is genetically ablated in mice, actin levels increase. Without desmin, some myofibers are disengaged from the Z-line, because low amounts of nebulette cannot stabilize an excess of actin filaments (Figure 10C). In this case, cellular backup mechanisms likely take over and involve the cytolinker plectin. Support for this idea comes from mouse studies of plectin isoforms (1f and 1d) showing that plectin is a major cytolinker connecting desmin to skeletal muscle costameres (Konieczny *et al.*, 2008).

Although investigating how desmin disease mutations affect the binding of nebulette to actin is important, future research should also focus on the dynamics of the desmin–nebulette–actin complex interaction in cardiomyocytes. Because Xin-repeat proteins also bind the nebulin/nebulette–actin complex, with temporally restricted interactions (Eulitz *et al.*, 2013), future work most likely will involve time-lapse microscopy images of the complex in live cardiomyocytes. Ultimately, studies focusing on desmin–nebulette temporal interactions will discern key mechanisms that involve actin dynamics.

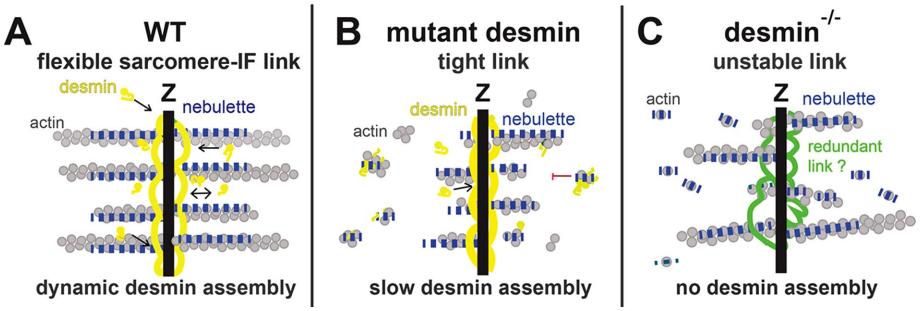

FIGURE 10: Nebulette highway connecting actin to DIFs in heart. This model states that nebulette coordinates the functional interplay of desmin and actin in cardiomyocytes. (A) Nebulette binds desmin oligomers and filaments (yellow) with high affinity. Nebulette (dashed blue line) stabilizes a short core of the actin filament extending ~150 nm out of the Z-line (gray circles). Desmin directly binds nebulette but does not bind directly to actin. (B) Mutant desmins linked to desminopathy (e.g., filament-forming mutations: E245D and T453I) bind nebulette with higher affinity than WT desmin, thus making it unavailable to stabilize actin filaments. A stickier mutant desmin binds nebulette, forming a tighter bond that retards filament elongation by trapping desmin oligomers. (C) Des$^{-/-}$ mice exhibit abnormally high levels of α-cardiac actin and improperly assembled nebulette on the actin filaments. Without desmin, a number of myofibers are disorganized, because low amounts of nebulette cannot properly stabilize an excess amount of actin.

MATERIALS AND METHODS

Ex vivo chick cardiomyocyte cell culture and cell lines

Six-day-old embryos were extracted from chicken eggs (purchased from Texas A&M, College Station, TX). Beating hearts were immediately digested in trypsin diluted in Hank's saline to dissociate cells from the heart tissue. Cells were plated at a density of 5×10^5 cells/ml in 35 mm cell-culture dishes on #1.5 coverslips (0.17 mm) in minimal essential media with Earle's salts (Hyclone; SH30244.01), supplemented with 5% fetal bovine serum, 2 mM L-glutamine, and 1% penicillin and streptomycin mix. To reduce fibroblast proliferation, cardiomyocytes were fed with media lacking L-glutamine. RD and Neuro2a cell lines were maintained following the ATCC instructions. The vimentin knockout fibroblast cell line was a kind gift from R. Goldman, Northwestern University, Chicago, IL.

Immunohistochemistry and nebulette signal image quantification

Three WT and 3 Des$^{-/-}$ hearts from 6-mo-old male mice were embedded in paraffin and sectioned for immunofluorescence analysis. The care and treatment of animals used in the study followed the institutional approved guidelines. Formalin-fixed, paraffin-embedded sections of normal canine heart and tongue were evaluated using immunofluorescence detection. Paraffin-embedded multitissue sections (~ 5 μm) were deparaffinized in xylene and rehydrated with graded alcohols. Heat-induced antigen retrieval was performed in a pressure cooker (Decloaker, Biocare Medical, Concord, CA) using citrate buffer at pH 6. The immunohistochemical procedure was performed using an automated platform (Dako, Carpinteria, CA). The total intensity of nebulette and desmin in stained-tissue images was quantified to determine the intensity value/pixel, and cumulative histogram distributions were generated using a LaTeX algorithm written by L. Macri (Texas A&M University, College Station, TX. The distance between nebulette striations was analyzed using the line tool in heart tissue sections stained for nebulette to generate line profiles using ImageJ (National Institutes of Health).

Immunofluorescence microscopy

Five-day-old ex vivo cardiomyocytes plated on coverglass #1.5 were washed in phosphate-buffered saline (PBS), relaxed (150 mM KCl, 5 mM $MgCl_2$, 10 mM MOPS, 1 mM EGTA, and 4 mM ATP, pH 7.4) for 15 min, fixed in 3% paraformaldehyde for 30 min at room temperature (RT), and rinsed three times with PBS. Before being stained, the cells were permeabilized in 0.2% Triton X-100 in PBS for 5 min and blocked in 1× PBS (2% bovine serum albumin [BSA] and 1% NGS) for 30 min at RT. The primary antibodies used were monoclonal desmin clone D33 (1:500; Dako; M0760), polyclonal anti-nebulette M4 (1:500; this study), and anti-mouse tropomyosin (1:50; Developmental Studies Hybridoma Bank). Fluorescent antibodies used to stain the tissue at 1:300 were Alexa Fluor rabbit 488, Alexa Fluor 594, or Alexa Fluor 647 (Life Technologies). The affinity-purified peptide rabbit antibody designed in this study against human nebulette peptide (C-Ahx-SYRKDVQDTH-TYSAELDRPD-amide), spanning amino acids 162–181, was selected both because of its predicted antigenic activity and reduced amino acid identity to nebulin. For staining nuclei, DAPI (4′, 6-diamidino-2-phenylindole, dihydrochloride at 1 ng/ml) diluted in water was used. The slides were mounted in Aqua Polymount (Polysciences, Warrington, PA) for wide-field and confocal imaging. For GSD superresolution microscopy images, cells were costained with nebulette M4 (1:300) and tropomyosin CH1 (1:10) or desmin D33 (1:300). For dual-color GSD superresolution images of ex vivo cardiomyocytes, nebulette was detected with Alexa Fluor 532 goat anti-rabbit immunoglobulin G (IgG; 1:200), and tropomyosin and desmin with Alexa Fluor 647 goat anti-mouse IgG (1:200; Life Technologies). The mounting of the slides was done 1 min before imaging. Fixed coverslips were maintained in PBS in a freshly mixed buffer containing β-mercaptoethanol and sealed carefully around the coverslip to avoid oxidation. Leica Confocal SPE and Leica SR GSD microscopes were used for all images presented in this study. Images were pseudocolored red, green, pink, yellow, and blue for presentation with Adobe Photoshop CS6. The region of interest obtained in each of the GSD images presented in this study is 18 × 18 μm, with a total of 900 pixels and approximately ~20 nm resolution per pixel.

Cloning

The N-terminal histidine (His)-tagged recombinant nebulette protein-affinity constructs cloned in this study were generated as follows: the plasmid encompassing modules 1–5 (M1–5) was amplified by PCR using Phusion high-fidelity polymerase (Finnzymes) as a *Bam*HI-*Eco*RI insert using 5′ and 3′ primers (5′-CGC GGA TCC CCT GTT ATT GAA GAC TTA AGC ATG-3′; 5′-CCG GAA TTC GTC TTC CAA TTA CAG CGG GCT-3′); the plasmid encompassing the amino terminal end of nebulette through module 6 (N-M6) was amplified as a *Bam*HI-*Eco*RI insert using 5′and 3′ primers (5′-CCG GAA TTC ATT AAC AAA CTC AAT GTA ATT CGC-3′; 5′-CGC GGA TCC ATG AGG GTC CCT GTA TTT GAG-3′). All these nebulette inserts were amplified from a pGEX4T-nebulette plasmid generously provided by C. Gregorio (University of Arizona). The PCR fragment was ligated into the corresponding *Bam*HI-*Eco*RI sites of the 6×His-tag

vector pET28a. The pIRES-His-nebulette M1–5 plasmid was cloned by subcloning the nebulette M1–5 *Bsp*EI-*Not*I insert using 5′ and 3′ primers (5′-GAG AGA TCC GGA CCT GTT ATT GAA GAC TTA AGC ATG-3′; 5′-GAG AGA GCG GCC GCG TCT TCC AAT TAC AGC GGG CT-3′) into pIRES-PURO3 HIS vector. The fidelity of the reading frames was verified by sequencing.

Protein purifications

BL21 (DE3) *Escherichia coli* was transformed into either pET-28a nebulette M1–5, pET-28a nebulette N-M6. Recombinant nebulette with an N-terminal His-tagged was purified using the 6×His-purification QIAexpressionist system (Qiagen). Modifications to the protocol as described below were shown to significantly optimize the recombinant nebulette protein yield. Before adding the lysis buffer, we dissolved a cOmplete ULTRA Tablet, Mini, EDTA-free (Roche), protease inhibitor cocktail into the lysis buffer. We also ensured complete lysis of the bacterial cells by using a tight-fitting dounce homogenizer (Sartorius, Germany). Following the homogenization step, we added Triton X-100 to equal 1% in solution. Batch chromatography proved to yield a higher purified protein concentration at the elution step. Coomassie brilliant blue (CBB)-stained SDS–PAGE gels and Western blots assessed protein yield and purity. WT and mutant desmin were purified from bacterial inclusion bodies followed by two ion-exchange chromatography columns, respectively (diethylaminoethyl [DEAE] and carboxymethyl [CM] sepharose fast flow; GE Healthcare Life Sciences), as previously described (Baker *et al*., 2013).

ELISAs

Triplicate wells in microtiter 96-well plates (BD Biosciences) were coated with 200 nM His-nebulette truncation protein as indicated in each experiment in 0.1 M carbonate buffer (pH 9.6) ON at 4°C. Wells were washed and blocked for 1 h with binding buffer (20 mM HEPES, pH 7.4, 80 mM KCl, 2 mM $MgCl_2$, 0.05% Tween-20, and 0.2% BSA). WT or mutant desmin was added to each in solution dissolved in binding buffer at concentrations ranging from 1 to 300 nM for 1 h at RT. After five washes with binding buffer, the plate was incubated with mouse monoclonal anti-desmin (Sigma; D1033) for 1 h. Following washes, anti-mouse horseradish peroxidase–conjugated antibody (Bio-Rad) was added for 1 h at RT. Dissolved substrate (2,2-azino-bis-3-ethylbenzothiazoline-6-sulfonic acid diammonium salt) (Sigma; A9941) in 0.05 M phosphate-citrate buffer (pH 5; Sigma P4809) was incubated for 30 min at 37°C. The binding interaction was determined by a colorimetric reaction at A_{405} on a BMG plate reader. The B_{max} and K_d values were determined using a one-site binding hyperbola nonlinear regression fit with GraphPad software.

Sucrose gradient cosedimentation ultracentrifugation assays

WT and mutant desmin were diluted to ~0.5 g/l and placed in dialysis tubing (50,000 MCWO, Spectrum Laboratories) in 8 M urea made in dialysis buffer (5 mM Tris, 1 mM EDTA, 0.1 mM EGTA, and 1 mM DTT; pH 8.4) for 20 min at RT. Proteins were subsequently serially dialyzed at RT in four dialysis buffers (containing 4, 2, 1, and 0 M urea) for 20 min each using a plate stirrer. Excess fresh dialysis buffer was used for ON dialysis at 4°C. Nebulette was dialyzed directly in dialysis buffer. Microaggregates in dialyzed nebulette preparation were removed by ultracentrifugation in a Beckman Airfuge at 100,000 × *g* (30 psi) for 30 min (Supplemental Figure 3) before starting this assay.

Protein concentrations were determined by Bradford assay (Bio-Rad Laboratories). The desired molar ratios were calculated and the assembly reactions were carried out as indicated in each experiment. Proteins were either layered onto a 0.85 M sucrose cushion or a 10–70% sucrose gradient in ultracentrifuge tubes, respectively (344090 or 344059; Coulter Beckman). Sedimentation was performed by ultracentrifugation using SW40 rotors at 28,000 rpm, respectively. The indicated fractions in each experiment were collected after 5 h ultracentrifugation and analyzed by SDS–PAGE. Gel band intensities of CBB G-250 stained gels were quantified using ImageJ software and analyzed as percentages of pellet samples. Proteins were renatured by dialysis (as described above). After samples were incubated at 37°C for 1 h and centrifuged at 100,000 × *g* for 30 min at 30 psi, aliquots were analyzed in 10% SDS–PAGE.

Coimmunoprecipitation assay

Ex vivo cardiomyocytes harvested from neonatal rats and embryonic chicks were plated on a 10-cm tissue culture dish at a 1×10^6/ml density. Three days after isolation, cell lysates were prepared in 500 µl of ice-cold RIPA buffer (150 mM NaCl, 1% NP-40, 0.1% SDS, 50 mM Tris-HCl, pH 8.0, and 0.5% sodium deoxycholate) supplemented with a freshly dissolved cocktail of PMSF and Pefabloc SC protease inhibitors. Cell monolayers were mechanically disrupted on ice; soluble lysates were collected and centrifuged for 15 min at 15,000 × *g*. Pellet fractions were dissolved in 8 M urea dissolved in 2× Laemmli buffer. As expected for an IF protein, up to ~90% of the endogenous desmin was found in the insoluble fraction (unpublished data). For lysates obtained from rat cardiomyocytes, ~2 µg/ml anti-desmin D9 (Dako) or nebulette M4 antibodies were coupled to protein A-magnetic bead slurry (100-02D; Dynal) following the manufacturer's instructions (Dynabeads Antibody coupling kit, Invitrogen; 143.11D). Soluble proteins in the cell-lysate supernatants were incubated in parallel, with magnetic beads coupled to either the desmin or the nebulette antibodies, ON at 4°C under constant rotation. For lysates obtained from chick cardiomyocytes, anti-desmin D76 ascites (Iowa Hybridoma Bank) were incubated with protein G-agarose beads (Pierce). After the beads were washed with 1× PBS containing 0.1% Triton X-100, using the magnetic holder to retrieve the bead–antibody–lysate complexes, the complexes were eluted 1× Laemmli buffer, boiled for 5 min, and analyzed by Western blot.

Western blots and band densitometry

Six 129SV mice (3 WT and 3 knockout) were perfused in PBS and their cardiac phenotypes were examined. All three desmin knockout hearts were fibrotic and had calcium scores between 1 and 2. For total protein extraction, hearts from 3-mo-old WT and $Des^{-/-}$ male mice were solubilized in 500 µl of SDS-lysis buffer (50 mM Tris-HCl, pH 6.7, 2% SDS, and 1 mM Na_3VO_4) supplemented with complete protease inhibitors (Roche). Seven to 10 ceramic Precellys beads (CK28L; 2.8 mm diameter; Peqlab) were added per sample. Tissues were homogenized twice for 30 s in a temperature-controlled Precellys 24. For removal of insoluble debris, evenly homogenized hearts were centrifuged for 15 min at 13,000 rpm at 4°C. Resuspended supernatants were boiled at 95°C for 5 min in 3× Laemmli buffer and stored at –80°C until use. Protein concentrations were determined using the Bradford assay (Bio-Rad) for each heart. The concentrations obtained ranged between 25 and 47 µg/ml. For Western blotting, equivalent amounts of proteins were run on SDS–PAGE gels, and proteins were transferred to polyvinylidene difluoride membranes (Immobilon). Blots were probed with the following antibodies: affinity-purified polyclonal rabbit peptide anti-nebulette M5 (this study), monoclonal mouse anti-desmin D9 (10519; Progen), mouse ascites anti–α-sarcomeric actin 5C5 immunoglobulin M (A2172; Sigma), mouse ascites anti–α-cardiac actin IgG1 (Ac1-20.4.2; Progen), rabbit anti–C-terminal vimentin, monoclonal mouse anti-GAPDH (G8795; Sigma).

Blot images were saved as 8-bit TIFFs, and the background was subtracted with a rolling-ball radius of 50 pixels with ImageJ. Using a rectangular tool, we drew equal areas on each band for analysis. Gaussian density plots for each band were quantified. The relative percentage for each fraction was normalized relative to the sum of all the gray values measured in the supernatant, sucrose, and pellet fractions. Values plotted show the means ± SD.

Transmission EM

Desmin was diluted to 0.1 g/l in 5 mM Tris-HCl (pH 8.4) buffer with or without nebulette and mounted on copper grids (Electron Microscopy Sciences; CF200-Cu-50). Samples were fixed for 10 s with 5 mM Tris-HCl (pH 8.4), 20 mM NaCl, and 0.1% glutaraldehyde. Excess proteins were carefully removed from the grid on the side using blotting paper. Grids were rinsed with 0.1 µm filtered dH_2O for 5 s, blotted again, negatively stained with 0.2% uryanyl acetate for 20 s, and blotted dry. Images were obtained using a Morgagni FEI transmission electron microscope.

Rheological viscometry assay

For reconstitution of the DIF tetramers, a stepwise serial dialysis was done as described above. Viscometry assays were used to quantitatively measure the relative viscosity (e.g., resistance of the desmin tetramers to flow) of desmin and the desmin mutant, E245D, in the presence and absence of nebulette. Ostwald semimicro viscometers (Cannon Instrument Company, State College, PA) were used to obtain measurements after the initiation of assembly upon addition of salt inside a 37°C transparent water bath. Before the experiment, the viscometers were soaked overnight in 3 M guanidine thiocyanate, rinsed 10 times with ddH_2O to remove any trace chemical, and dried with a vacuum hose. A Bradford protein assay was used to determine protein concentration. The protein concentration was adjusted with Tris-HCl buffer to 0.1 g/l for desmin and 0.01 g/l for nebulette in the bulk solution. WT or mutant desmin and nebulette were mixed sequentially before the addition of assembly buffer. Assembly of the protein samples was initiated with 10× low-assembly buffer (50 mM NaCl in 20 mM Tris-HCl, pH 7.0) at 37°C. We measured fall times for the dialysis buffer (control) and the bulk solution every min for 30 min to obtain the relative-viscosity profile. We used GraphPad Prism 5.2 software (San Diego, CA) to plot and obtain nonlinear curve fits for each data set. Each experiment was repeated independently three times, and plots are normalized averages ± SDs.

ACKNOWLEDGMENTS

Thanks to Y. Coronado, K. Timberlake, L. Baker, D. Gillis, A. Ambrus, and P. Zugschwerdt for their expert technical assistance. We thank S. Papathanasiou for dissecting mouse hearts, R. Bauer for providing rat cardiomyocytes, and C. Gregorio for the kind gift of GST-nebulette plasmid. We are very grateful to D. Conover for editorial help. The American Heart Association funded this research (grant number 2110057 to G.M.C.). H.H. was supported by the German Research Foundation (DFG HE 1853/9-2, FOR 1228). We dedicate this work to the families grieving loved ones lost because of cardiac sudden death.

REFERENCES

Arbustini E, Pasotti M, Pilotto A, Pellegrini C, Grasso M, Previtali S, Repetto A, Bellini O, Azan G, Scaffino M, *et al.* (2006). Desmin accumulation restrictive cardiomyopathy and atrioventricular block associated with desmin gene defects. Eur J Heart Fail 8, 477–483.

Arimura T, Nakamura T, Hiroi S, Satoh M, Takahashi M, Ohbuchi N, Ueda K, Nouchi T, Yamaguchi N, Akai J, *et al.* (2000). Characterization of the human nebulette gene: a polymorphism in an actin-binding motif is associated with nonfamilial idiopathic dilated cardiomyopathy. Hum Genet 107, 440–451.

Baker LK, Gillis DC, Sharma S, Ambrus A, Herrmann H, Conover GM (2013). Nebulin binding impedes mutant desmin filament assembly. Mol Biol Cell 24, 1918–1932.

Bang ML, Chen J (2015). Roles of nebulin family members in the heart. Circ J 79, 2081–2087.

Bang ML, Gregorio C, Labeit S (2002). Molecular dissection of the interaction of desmin with the C-terminal region of nebulin. J Struct Biol 137, 119–127.

Bang ML, Li X, Littlefield R, Bremner S, Thor A, Knowlton KU, Lieber RL, Chen J (2006). Nebulin-deficient mice exhibit shorter thin filament lengths and reduced contractile function in skeletal muscle. J Cell Biol 173, 905–916.

Bar H, Mucke N, Kostareva A, Sjoberg G, Aebi U, Herrmann H (2005). Severe muscle disease-causing desmin mutations interfere with in vitro filament assembly at distinct stages. Proc Natl Acad Sci USA 102, 15099–15104.

Bar H, Schopferer M, Sharma S, Hochstein B, Mucke N, Herrmann H, Willenbacher N (2010). Mutations in desmin's carboxy-terminal "tail" domain severely modify filament and network mechanics. J Mol Biol 397, 1188–1198.

Bar H, Strelkov SV, Sjoberg G, Aebi U, Herrmann H (2004). The biology of desmin filaments: how do mutations affect their structure, assembly, and organisation? J Struct Biol 148, 137–152.

Bonzo JR, Norris AA, Esham M, Moncman CL (2008). The nebulette repeat domain is necessary for proper maintenance of tropomyosin with the cardiac sarcomere. Exp Cell Res 314, 3519–3530.

Capetanaki Y, Papathanasiou S, Diokmetzidou A, Vatsellas G, Tsikitis M (2015). Desmin related disease: a matter of cell survival failure. Curr Opin Cell Biol 32, 113–120.

Cherepanova O, Orlova A, Galkin VE, van der Ven PF, Furst DO, Jin JP, Egelman EH (2006). Xin-repeats and nebulin-like repeats bind to F-actin in a similar manner. J Mol Biol 356, 714–723.

Chernyatina AA, Guzenko D, Strelkov SV (2015). Intermediate filament structure: the bottom-up approach. Curr Opin Cell Biol 32, 65–72.

Chu M, Gregorio CC, Pappas CT (2016). Nebulin, a multi-functional giant. J Exp Biol 219, 146–152.

Claeys KG, Fardeau M (2013). Myofibrillar myopathies. Handb Clin Neurol 113, 1337–1342.

Clemen CS, Herrmann H, Strelkov SV, Schroder R (2013). Desminopathies: pathology and mechanisms. Acta Neuropathol 125, 47–75.

Conover GM, Gregorio CC (2011). The desmin coil 1B mutation K190A impairs nebulin Z-disc assembly and destabilizes actin thin filaments. J Cell Sci 124, 3464–3476.

Conover GM, Henderson SN, Gregorio CC (2009). A myopathy-linked desmin mutation perturbs striated muscle actin filament architecture. Mol Biol Cell 20, 834–845.

Esham M, Bryan K, Milnes J, Holmes WB, Moncman CL (2007). Expression of nebulette during early cardiac development. Cell Motil Cytoskeleton 64, 258–273.

Eulitz S, Sauer F, Pelissier MC, Boisguerin P, Molt S, Schuld J, Orfanos Z, Kley RA, Volkmer R, Wilmanns M, *et al.* (2013). Identification of Xin-repeat proteins as novel ligands of the SH3 domains of nebulin and nebulette and analysis of their interaction during myofibril formation and remodeling. Mol Biol Cell 24, 3215–3226.

Fawcett DW, Bloom W (1986). A Textbook of Histology, Philadelphia: Saunders.

Gonsior SM, Gautel M, Hinssen H (1998). A six-module human nebulin fragment bundles actin filaments and induces actin polymerization. J Muscle Res Cell Motil 19, 225–235.

Granger BL, Lazarides E (1978). The existence of an insoluble Z disc scaffold in chicken skeletal muscle. Cell 15, 1253–1268.

Granger BL, Lazarides E (1979). Desmin and vimentin coexist at the periphery of the myofibril Z disc. Cell 18, 1053–1063.

Herrmann H, Aebi U (2004). Intermediate filaments: molecular structure, assembly mechanism, and integration into functionally distinct intracellular scaffolds. Annu Rev Biochem 73, 749–789.

Herrmann H, Haner M, Brettel M, Ku NO, Aebi U (1999). Characterization of distinct early assembly units of different intermediate filament proteins. J Mol Biol 286, 1403–1420.

Herrmann H, Kreplak L, Aebi U (2004). Isolation, characterization, and in vitro assembly of intermediate filaments. Methods Cell Biol 78, 3–24.

Holmes WB, Moncman CL (2008). Nebulette interacts with filamin C. Cell Motil Cytoskeleton 65, 130–142.
Holtzer H, Bennett GS, Tapscott SJ, Croop JM, Toyama Y (1982). Intermediate-size filaments: changes in synthesis and distribution in cells of the myogenic and neurogenic lineages. Cold Spring Harb Symp Quant Biol 46, 317–329.
Jackson S, Schaefer J, Meinhardt M, Reichmann H (2015). Mitochondrial abnormalities in the myofibrillar myopathies. Eur J Neurol 22, 1429–1435.
Jin JP, Wang K (1991). Cloning, expression, and protein interaction of human nebulin fragments composed of varying numbers of sequence modules. J Biol Chem 266, 21215–21223.
Kazmierski ST, Antin PB, Witt CC, Huebner N, McElhinny AS, Labeit S, Gregorio CC (2003). The complete mouse nebulin gene sequence and the identification of cardiac nebulin. J Mol Biol 328, 835–846.
Konieczny P, Fuchs P, Reipert S, Kunz WS, Zeold A, Fischer I, Paulin D, Schroder R, Wiche G (2008). Myofiber integrity depends on desmin network targeting to Z-disks and costameres via distinct plectin isoforms. J Cell Biol 181, 667–681.
Kornreich M, Avinery R, Malka-Gibor E, Laser-Azogui A, Beck R (2015). Order and disorder in intermediate filament proteins. FEBS Lett 589, 2464–2476.
Koster S, Weitz DA, Goldman RD, Aebi U, Herrmann H (2015). Intermediate filament mechanics in vitro and in the cell: from coiled coils to filaments, fibers and networks. Curr Opin Cell Biol 32, 82–91.
Littlefield RS, Fowler VM (2008). Thin filament length regulation in striated muscle sarcomeres: pointed-end dynamics go beyond a nebulin ruler. Semin Cell Dev Biol 19, 511–519.
Li B, Zhuang L, Trueb B (2004). Zyxin interacts with the SH3 domains of the cytoskeletal proteins LIM-nebulette and Lasp-1. J Biol Chem 279, 20401–20410.
Maiellaro-Rafferty K, Wansapura JP, Mendsaikhan U, Osinska H, James JF, Taylor MD, Robbins J, Kranias EG, Towbin JA, Purevjav E (2013). Altered regional cardiac wall mechanics are associated with differential cardiomyocyte calcium handling due to nebulette mutations in preclinical inherited dilated cardiomyopathy. J Mol Cell Cardiol 60, 151–160.
Mastrototaro G, Liang X, Li X, Carullo P, Piroddi N, Tesi C, Gu Y, Dalton ND, Peterson KL, Poggesi C, *et al.* (2015). Nebulette knockout mice have normal cardiac function, but show Z-line widening and up-regulation of cardiac stress markers. Cardiovasc Res 107, 216–225.
Milner DJ, Mavroidis M, Weisleder N, Capetanaki Y (2000). Desmin cytoskeleton linked to muscle mitochondrial distribution and respiratory function. J Cell Biol 150, 1283–1298.
Milner DJ, Weitzer G, Tran D, Bradley A, Capetanaki Y (1996). Disruption of muscle architecture and myocardial degeneration in mice lacking desmin. J Cell Biol 134, 1255–1270.
Moncman CL, Wang K (1995). Nebulette: a 107 kD nebulin-like protein in cardiac muscle. Cell Motil Cytoskeleton 32, 205–225.
Moncman CL, Wang K (1999). Functional dissection of nebulette demonstrates actin binding of nebulin-like repeats and Z-line targeting of SH3 and linker domains. Cell Motil Cytoskeleton 44, 1–22.
Moncman CL, Wang K (2000). Architecture of the thin filament-Z-line junction: lessons from nebulette and nebulin homologies. J Muscle Res Cell Motil 21, 153–169.
Moncman CL, Wang K (2002). Targeted disruption of nebulette protein expression alters cardiac myofibril assembly and function. Exp Cell Res 273, 204–218.
Ogut O, Hossain MM, Jin JP (2003). Interactions between nebulin-like motifs and thin filament regulatory proteins. J Biol Chem 278, 3089–3097.
Omary MB (2009). "IF-pathies": a broad spectrum of intermediate filament-associated diseases. J Clin Invest 119, 1756–1762.
Pappas CT, Bliss KT, Zieseniss A, Gregorio CC (2011). The nebulin family: an actin support group. Trends Cell Biol 21, 29–37.
Perrot A, Tomasov P, Villard E, Faludi R, Melacini P, Lossie J, Lohmann N, Richard P, De Bortoli M, Angelini A, *et al.* (2016). Mutations in NEBL encoding the cardiac Z-disk protein nebulette are associated with various cardiomyopathies. Arch Med Sci 12, 263–278.
Purevjav E, Varela J, Morgado M, Kearney DL, Li H, Taylor MD, Arimura T, Moncman CL, McKenna W, Murphy RT, *et al.* (2010). Nebulette mutations are associated with dilated cardiomyopathy and endocardial fibroelastosis. J Am Coll Cardiol 56, 1493–1502.
Schaffeld M, Herrmann H, Schultess J, Markl J (2001). Vimentin and desmin of a cartilaginous fish, the shark *Scyliorhinus stellaris*: sequence, expression patterns and in vitro assembly. Eur J Cell Biol 80, 692–702.
Strach K, Sommer T, Grohe C, Meyer C, Fischer D, Walter MC, Vorgerd M, Reilich P, Bar H, Reimann J, *et al.* (2008). Clinical, genetic, and cardiac magnetic resonance imaging findings in primary desminopathies. Neuromuscul Disord 18, 475–482.
Tonino P, Pappas CT, Hudson BD, Labeit S, Gregorio CC, Granzier H (2010). Reduced myofibrillar connectivity and increased Z-disk width in nebulin-deficient skeletal muscle. J Cell Sci 123, 384–391.
van Spaendonck-Zwarts KY, van Hessem L, Jongbloed JD, de Walle HE, Capetanaki Y, van der Kooi AJ, van Langen IM, van den Berg MP, van Tintelen JP (2011). Desmin-related myopathy. Clin Genet 80, 354–366.
Vrabie A, Goldfarb LG, Shatunov A, Nagele A, Fritz P, Kaczmarek I, Goebel HH (2005). The enlarging spectrum of desminopathies: new morphological findings, eastward geographic spread, novel exon 3 desmin mutation. Acta Neuropathol 109, 411–417.
Wang X, Osinska H, Gerdes AM, Robbins J (2002). Desmin filaments and cardiac disease: establishing causality. J Card Fail 8, S287–292.
Wang K, Ramirez-Mitchell R (1983). A network of transverse and longitudinal intermediate filaments is associated with sarcomeres of adult vertebrate skeletal muscle. J Cell Biol 96, 562–570.
Yamamoto DL, Vitiello C, Zhang J, Gokhin DS, Castaldi A, Coulis G, Piaser F, Filomena MC, Eggenhuizen PJ, Kunderfranco P, *et al.* (2013). The nebulin SH3 domain is dispensable for normal skeletal muscle structure but is required for effective active load bearing in mouse. J Cell Sci 126, 5477–5489.